Multirate Forward-model Disturbance Observer for Feedback Regulation beyond Nyquist Frequency

Xu Chen[a,*], Hui Xiao[a]

[a]*Department of Mechanical Engineering, University of Connecticut, Storrs, CT, 06269, USA.*

Abstract

A fundamental challenge in digital control arises when the controlled plant is subjected to a fast disturbance dynamics but is only equipped with a relatively slow sensor. Such intrinsic difficulties are, however, commonly encountered in many novel applications such as laser- and electron-beam-based additive manufacturing, human-machine interaction, etc. This paper provides a discrete-time regulation scheme for exact sampled-data rejection of disturbances beyond Nyquist frequency. By introducing a model-based multirate predictor and a forward-model disturbance observer, we show that the inter-sample disturbances can be fully attenuated despite the limitations in sampling and sensing. The proposed control scheme offers several advantages in stability assurance and lucid design intuitions. Verification of the algorithm is conducted on a motion control platform that shares the general characteristics in several advanced manufacturing systems.

Keywords: digital control, disturbance beyond Nyquist frequency, disturbance rejection, disturbance observer

1. Introduction

A fundamental challenge arises in feedback control if the sampling of the output is not fast enough to capture the major frequency components of the disturbances—or more specifically, when significant disturbances occur beyond Nyquist frequency. Such a scenario is, however, becoming increasingly important in modern control systems, due to, on the one hand the continuous pursuit of higher performance and robustness using slow or limited sensing mechanisms (e.g., vision servo, chemical process, human-machine interaction, etc); and on the other hand, many hardware constrains in novel applications such as in-situ sensing in additive manufacturing [1] and intrinsic numerical limitations [2] in ultra fast sampling. In these applications and the like, significant disturbances beyond Nyquist frequency are unattended under conventional servo design. Such large intersample/hidden disturbances are extremely dangerous, as they cause unobserved performance loss in the actual system, increase system fatigue, and can even lead to hardware failures. As a particular example, for advanced manufacturing such as the laser-based additive manufacturing process [1], there are significant challenges and opportunities for high-speed high-precision sensing and metrology. For instance, [3, 4] used an infrared camera for the sensing and control of the molten-pool profile in laser cladding. The dynamics of laser melting is very fast. Although using a high-speed camera at 800 frames per second, the control of the closed-loop is limited at 30 Hz, as it takes time for the raw image data to be processed and for the signature characteristics in the molten pool to be estimated. Overcoming the limitations from slow/limited sampling is thus key for unlocking the full potentials of performance and robustness in the next-generation additive manufacturing.

From the viewpoint of information recovery, the pioneering work of Shannon [5]—now covered in standard text books such as [6]—has shown that in order for the original analog information to be fully recovered from its samples, (i) the analog signal must be perfectly band-limited below Nyquist frequency, and (ii) an ideal lowpass filter (acausal and not interpretable using a transfer function) is available in the reconstruction process. Recent advances using sampled-data H_∞ theory has investigated broadband reconstruction to approximate the ideal digital-to-analog converter (DAC) [7]. Although perfect recovery is still theoretically not feasible, the H_∞ approach provides an optimal tool focusing on the actual analog performance. For other approximate reconstructions, one is referred to the survey in [8].

From the viewpoint of control design, multirate control and advanced DAC have been the main tools for tracking and regulation beyond Nyquist frequency. Let the plant output be sampled at T_s sec. Reference [9] introduced a multirate feedforward control for exact tracking of the reference at the T_s-sampled instances. Optimization-based multirate iterative learning control with consideration of the inter-sample behavior was discussed in [10]. In feedback algorithms, partial compensation and control of the inter-sample system behaviors have been investigated. [11] used generalized predictive control under quadratic cost functions on hard disk drive systems; asynchronized sampling and generalized holders were applied to improve the inter-sample behavior in repetitive control [12]; and [13] discussed beyond-Nyquist servo control via peak filters that are discretized at a sampling time smaller than T_s. Along the direction of changing the DAC, generalized sample hold

*Corresponding author.

Email addresses: xchen@uconn.edu (Xu Chen), hui.xiao@uconn.edu (Hui Xiao)

control has shown to be promising in sampled-data performance. However, the technique also has fundamental limitations in closed-loop robustness and sensitivity, which raised intrinsic difficulties for implementation in practice [14]. The introduction of the lifting technique [15] has been a major enabler for analysis of the inter-sample behavior. Under this scope, the challenge of inter-sample ripples has been shown to occur due to non-uniform gains of the discrete lifted system and inverse lifting [16, 17]. A synthesis based on lifting and internal model principle is provided in [18], where the internal model is embedded in a H_∞ synthesis to certify the continuous-time performance.

The goal of this paper is to introduce a shifted paradigm that goes beyond the acausal, non-ideal information recovery and partial feedback disturbance compensation. We provide a mixed-rate feedback solution for the missing piece of exact disturbance rejection at frequencies beyond the Nyquist limitation. This is achieved by the introduction of a multirate forward-model disturbance observer (MR-FMDOB) that enables full rejection of structured disturbances at both the sampling and any uniformly spaced inter-sample instances. Built on top of a baseline controller at the regular sampling time of T_s, such an exact compensation scheme constructs an internal feedback loop implemented at a higher sampling rate, where the inter-sample signals are constructed with model-based prediction using the slow T_s-sampled data. Integrating features of all-stabilizing parameterization [19, 20], the internal add-on loop guarantees the overall closed-loop stability and offers the convenience of being decoupled from the design of the baseline sub-Nyquist controller. Similar to [18], an internal model of the disturbance is implicitly integrated in the inner loop. The major differences here are the decoupled design of the fast-rate MR-FMDOB from the slow-rate baseline feedback control, and the all-stabilizing based observer structure that preserves features of the baseline servo. These properties enable additional design features such as adaptive control in the baseline or the multirate compensator, and are also useful for applications where the existing baseline servo has special features that are required to be preserved.

Notations: $\mathbb{R}$ denotes the set of real numbers. $\mathbb{Z}$ and $\mathbb{Z}^+$ denote, respectively, the sets of integers and positive integers. We use $x[n]$ and $x_c(t)$ to represent a discrete sequence and a continuous-time signal, respectively. $\mathscr{H}$ denotes a zero order hold (ZOH) whose transfer function is $H(s) = (1-\mathrm{e}^{-sT_s})/s$, if the sampling time is T_s.

2. Problem Formulation

Consider the system in Fig. 1, where the solid and dashed lines represent, respectively, continuous- and discrete-time signal flows. The main elements here include the continuous-time plant $P_c(s)$, the sampler $\mathscr{S}$ at a sampling time of T_s sec, the discrete-time controller $C(z)$, and the signal holder $\mathscr{H}$. Given the common hardware complication and the theoretical limitation [14] of generalized hold functions, we assume that the DAC implements a ZOH throughout the paper.

Throughout the paper, we assume that the plant has no hidden modes and the closed loop satisfies the nonpathological sampling condition [21]:

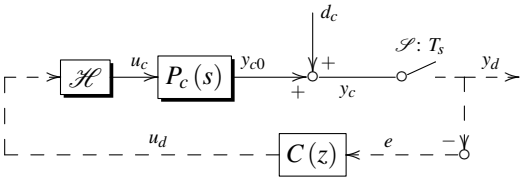

Figure 1: Block diagram of a sampled-data control system.

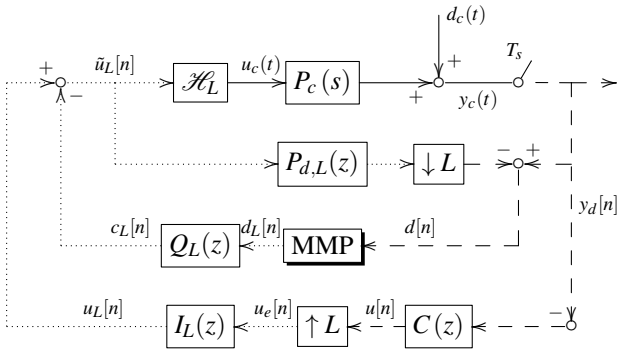

Figure 2: The proposed multirate disturbance rejection scheme.

Assumption 1. *$P_c(s) = P_0(s)\mathrm{e}^{-s\tau}$ where $\tau \geq 0$; $P_0(s)$ and $C(z)$ are both linear time invariant (LTI), irreducible, proper, and rational.*

Assumption 2. *(nonpathological sampling) Let the minimal state equation of the plant be $\dot{x} = Ax + Bu_c$. Take any two eigenvalues λ_i and λ_j of A, with $\mathbf{Re}(\lambda_i) = \mathbf{Re}(\lambda_j)$. It is assumed that $\mathbf{Im}(\lambda_i) - \mathbf{Im}(\lambda_j) \neq 2\pi p/T_s$ for any nonzero integer p.*

Under Assumption 2, sampling preserves controllability and observability, and the closed-loop sampled-data system is stable if and only if the discrete-time closed loop consisting of $C(z)$ and the ZOH equivalent of $P_c(s)$ is stable (see, e.g. [22, 23, 24]).

The focused problem is as follows. Suppose an additional fictitious faster sensor, at a sampling time of $T_s^{'} = T_s/L$ ($L \in \mathbb{Z}^+$), is available between y_c and $\mathscr{S}$ in Fig. 1. We provide a control algorithm such that $y_c(nT_s^{'})$ ($n \in \mathbb{Z}$) asymptotically converges to zero in the presence of a disturbance with significant spectrum beyond the Nyquist frequency $[1/(2T_s)$ Hz].

3. Main Results

Fig. 2 shows the proposed servo scheme for disturbance rejection beyond Nyquist frequency. Two groups of discrete signals are present, with their different sampling rates indicated by the dashed (slower) and dotted (faster) signal flows.

In the block diagram, the upsampler (between $u[n]$ and $u_e[n]$) and the interpolator $I_L(z)$ generate a fast signal $u_L[n]$ at a sampling time of T_s/L. Under a ZOH interpolator, $u_L[n] = u[n/L]$ when $n = 0, \pm L, \pm 2L, \ldots$ and $u_L[n] = u[k]$ when $kL < n < (k+1)L$, respectively. The upsampled signal then passes through $\mathscr{H}_L$, a T_s/L-based ZOH, with a transfer function $H_L(s) = (1-\mathrm{e}^{-sT_s/L})/s$.

The beyond-Nyquist disturbance rejection consists of two fast-sampling transfer functions $Q_L(z)$ and $P_{d,L}(z)$, a downsampling operator, and a multirate model-based predictor (MMP) inbetween the downsampler and $Q_L(z)$. In the subsequent derivations, we show that although $y_d[n]$ only contains information sampled at T_s, the inter-sample information in $d_c(t)$ can be fully reconstructed with MMP in Fig. 2, if $d_c(t)$ satisfies a disturbance model; and in that case, $c_L[n]$—the output of $Q_L(z)$—can fully remove the effect of the beyond-Nyquist sampled disturbance at a fast sampling period of T_s/L.

3.1. Multirate Forward-model Disturbance Observer

If the sampling time in Fig. 2 were T_s/L, the focused signal is the sampled output, and the downsampler and the MMP block were removed, then the top part of the block diagram is equivalent to the structure in Fig. 3. Here, $P_{d,L}(z)$ is the ZOH equivalent of $P_c(s)$, with a fast sampling time T_s/L; $d_L[n](\triangleq d_c(nT_s/L))$ and $y_L[n]$ are the T_s/L–sampled disturbance and the plant output, respectively.

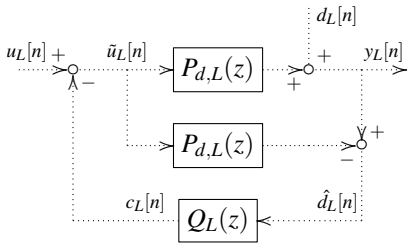

Figure 3: The proposed forward-model disturbance observer.

The disturbance compensation structure is branched from internal model control (IMC) [25], a special case of Youla-Kucera/all-stabilizing parameterization [26]. Compared with a standard IMC, the major difference here is that $u_L[n]$—the command external to the local feedback loop—is injected before the plant instead of serving as a reference before $Q_L(z)$. The resulting output satisfies, after some block-diagram algebra,

$$Y_L(z) = P_{d,L}(z)U_L(z) + (1 - P_{d,L}(z)Q_L(z))D_L(z), \qquad (1)$$

where the relationship between $u_L[n]$ and the output remains intact as if the local feedback does not exist; and additional dynamics is introduced between $d_L[n]$ and $y_L[n]$. The first property allows the design of the local feedback to be separated from that of the baseline control command $u_L[n]$. In other words, the design of $Q_L(z)$ is decoupled from that of $C(z)$ in Fig. 2. The second property enables a disturbance estimation and cancellation scheme. In more details, with the forward plant model in the center of Fig. 3, block diagram analysis gives that the input to $Q_L(z)$ is

$$Y_L(z) - P_{d,L}(z)\tilde{U}_L(z) = \Big(\cancel{P_{d,L}(z)\tilde{U}_L(z)} + D_L(z)\Big) \cancel{- P_{d,L}(z)\tilde{U}_L(z)},$$

i.e. $d_L[n]$ in time domain. This disturbance estimation is then processed by the cancellation filter $Q_L(z)$ to be discussed in the remainder of this subsection. Based on the above intuitions, we will hereafter refer to the proposed scheme in Fig. 3 the forward-model disturbance observer (FMDOB).

Remark 1. *We have modeled the disturbance to enter at the output side of the plant. For the case with $\tilde{d}(t)$ entering as the input of the plant, an equivalent output disturbance can be constructed. The analogy is valid as long as the plant does not have zeros that can annihilate the input disturbance. For a more detailed discussion on characterizing the locations of the disturbance, we refer interested readers to [27].*

The FMDOB has the same characteristic equation as IMC, since changing the allocation of input signals does not alter closed-loop stability. Hence FMDOB shares the same advantageous property of guaranteed stability as in IMC [25], if $Q_L(z)$ and $P_{d,L}(z)$ are stable.

Remark 2. *When combined with the baseline feedback design, $P_{d,L}(z)$—if unstable—is stabilized by $C(z)$.*

With the stability property and the decoupled design principle, we now use the affine Q parameterization $1 - P_{d,L}(z)Q_L(z)$ to design $Q_L(z)$ for disturbance rejection. Observe the structure of $1 - P_{d,L}(z)Q_L(z)$. To achieve an exact rejection of the disturbance at a particular frequency ω_o in (1), it must be that

$$1 - P_{d,L}(e^{j\omega_o})Q_L(e^{j\omega_o}) = 0. \qquad (2)$$

Let φ be the phase of $P_{d,L}(e^{j\omega_o})$ at ω_o. (2) is equivalent to:

$$|Q_L(e^{j\omega_o})| = \frac{1}{|P_{d,L}(e^{j\omega_o})|},\ \text{phase}(Q_L(e^{j\omega_o})) = -\varphi. \qquad (3)$$

In other words, $Q_L(e^{j\omega_o}) = P_{d,L}(e^{j\omega_o})^{-1}$ so that $Q_L(z)$ inverts the dynamics of $P_{d,L}(z)$ at ω_o.[1] Recall that $Q_L(z)$ must be stable. Certainly, unless for special minimum-phase plants with a relative degree of zero, it is not feasible to always assign an exact full inversion $P_{d,L}(z)^{-1}$ to $Q(z)$ due to instability and non-properness. In addition, when $\omega \neq \omega_o$, the magnitude of $1 - P_{d,L}(e^{j\omega})Q_L(e^{j\omega})$ must be maintained small to avoid amplification of other components in $d_L[n]$. The following proposition achieves a point-wise stable inversion while providing the needed small gain to $|1 - P_{d,L}(e^{j\omega})Q_L(e^{j\omega})|$ for $\omega \neq \omega_o$.

Proposition 1. *Let $1/(2T_s) < \Omega_o < L/(2T_s)$ (in Hz) and $\omega_o = 2\pi\Omega_o T_s/L$ be the frequency of a major disturbance component beyond the baseline Nyquist frequency, $1/(2T_s)$ Hz, in Fig. 2. Let $\varphi = \text{phase}(P_{d,L}(e^{j\omega_o}))$ be the phase response of the T_s/L–sampled discrete-time plant at ω_o; and assume that $P_{d,L}(e^{j\omega_o}) \neq 0$ (otherwise no feedback design can achieve the disturbance rejection). Let*

$$Q_L(z) = gQ_o(z)(b_0 + b_1 z^{-1}), \qquad (4)$$

with $g \in [0,1]$, and

$$b_0 = \frac{\cos\varphi - \sin\varphi\cot\omega_o}{|P_{d,L}(e^{j\omega_o})|},\ b_1 = \frac{1}{|P_{d,L}(e^{j\omega_o})|}\frac{\sin\varphi}{\sin\omega_o}; \qquad (5)$$

$$Q_o(z) = \frac{1}{2}\frac{(1-k_2)(1+z^{-1})(1-z^{-1})}{1+k_1(1+k_2)z^{-1}+k_2z^{-2}},\ k_1 = -\cos\omega_o. \qquad (6)$$

Then

[1] We assume that the plant does not have a null gain at ω_o.

1. $1-P_{d,L}(z)Q_L(z)$ *in (1) equals* $1-g\overset{g=1}{=}0$ *at* ω_o *and can be controlled to have almost unity gain at other frequencies—in other words, the feedback system in Fig. 3 fully rejects all disturbances at* ω_o *at the sampling instances when* $g=1$*, while maintaining the system dynamics at other frequencies.*
2. *Amplification at* $\omega\neq\omega_o$*, if any, is controlled by choosing*

$$k_2=\frac{1-\tan(\frac{\pi B_w T_s}{L})}{1+\tan(\frac{\pi B_w T_s}{L})} \tag{7}$$

and g, where B_w *(in Hz) is the 3-dB disturbance-rejection bandwidth of* $Q_o(z)$ *centered around* ω_o*.*
3. *The overall magnitude of* $1-P_{d,L}(e^{j\omega})Q_L(e^{j\omega})$ *satisfies*

$$\int_0^{\pi}\ln|1-P_{d,L}(e^{j\omega})Q_L(e^{j\omega})|d\omega = \pi\left(\sum_{i=1}^{n_\gamma}\ln|\gamma_i|-\ln|\sigma+1|\right), \tag{8}$$

where $\{\gamma_i\}_{i=1}^{n_\gamma}$ *(*$n_\gamma\geq 0$*) is the set of unstable zeros of* $1-P_{d,L}(z)Q_L(z)$ *(*$\{\gamma_i\}_{i=1}^{n_\gamma}\triangleq\phi$ *if* $n_\gamma=0$*), and*

$$\sigma=\lim_{z\to\infty}P_{d,L}(z)Q_L(z)/(1-P_{d,L}(z)Q_L(z)).$$

Proof $Q_o(z)$ in (6) is a lattice-based band-pass filter whose bandwidth $B_{w,r}$ in radian is related to k_2 [28, 29], by

$$k_2=[1-\tan(B_{w,r}/2)]/[1+\tan(B_{w,r}/2)]. \tag{9}$$

At the sampling time of T_s/L, $B_{w.r}$ and B_w (in Hz) is related by $B_{w,r}=2\pi B_w T_s/L$. Substituting the relationship in (9) gives (7).

By definition (6), one can show that $Q_o(e^{j\omega_o})=1$ at the center frequency ω_o. Hence from (4), $Q_L(e^{j\omega_o})=g(b_0+b_1e^{-j\omega_o})$. Equation (3), the condition of exact disturbance rejection, is then equivalent to

$$|b_o+b_1e^{-j\omega_o}|=\frac{1}{|P_{d,L}(e^{j\omega_o})|}, \tag{10}$$

$$\text{phase}(b_o+b_1e^{-j\omega_o})=-\varphi. \tag{11}$$

Solving the equation set yields (5). The above results give that $|Q_L(e^{j\omega_o})|=g/|P_{d,L}(e^{j\omega_o})|$, and that the phase of $Q_L(e^{j\omega_o})$ equals $-\varphi$. Hence, $1-P_{d,L}(e^{j\omega_o})Q_L(e^{j\omega_o})=1-g\overset{g=1}{=}0$, which proves the asserted disturbance rejection at ω_o.

Outside the passband when $|Q_o(e^{j\omega})|\ll 1$, we have $1-P_{d,L}(e^{j\omega})Q_L(e^{j\omega})\approx 1$. The approximation sign here can be made arbitrarily close to equality, by reducing the bandwidth of $Q_o(e^{j\omega})$. From (1), the dynamics of the feedback loop then recovers to the case without FMDOB.

For Fig. 3, the loop transfer function, with the loop cut open as shown below

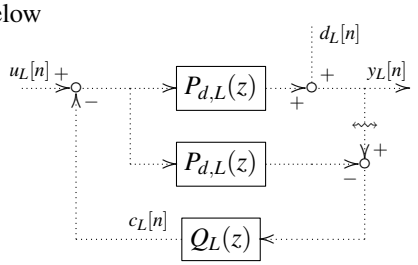

is $L_L(z)=P_{d,L}(z)Q_L(z)/(1-P_{d,L}(z)Q_L(z))$. Based on Bode's Integral Theorem (see, e.g. [30]),

$$\int_0^{\pi}\ln\left|\frac{1}{1+L_L(e^{j\omega})}\right|d\omega=\pi\left(\sum_{i=1}^{n_\gamma}\ln|\gamma_i|-\ln|\sigma+1|\right), \tag{12}$$

where γ_i's are the $n_\gamma(\geq 0)$ unstable poles of $L_L(z)$ and $\sigma=\lim_{z\to\infty}L_L(z)$. Substituting the formula of $L_L(z)$ gives the third asserted result in the proposition. □

Recall (1). Given a target frequency ω_o, the frequency-domain property of the proposed $Q_L(z)$ yields

$$Y_L(e^{j\omega})=\begin{cases}P_{d,L}(e^{j\omega})U_L(e^{j\omega}), & \omega=\omega_o\\ P_{d,L}(e^{j\omega})U_L(e^{j\omega})+D_L(e^{j\omega}), & \omega\neq\omega_o\end{cases}. \tag{13}$$

The first equality in (13) provides the desired disturbance rejection. Although the same mathematical relationship is achieved if one had assigned $Q_o(z)=1$, the latter design is sensitive to the practically inevitable noises in $d_L[n]$. By designing the band-pass $Q_o(z)$ in (6), robustness is added to the algorithm, such that the second equality in (13) holds, to avoid amplification of $D_L(e^{j\omega})$ if $\omega\neq\omega_o$.

Remark 3. *In (8), for strictly proper plants,* $\lim_{z\to\infty}P_{d,L}(z)=0$ *and* $\sigma=0$*. (8) simplifies to* $\int_0^{\pi}\ln|1-P_{d,L}(e^{j\omega})Q_L(e^{j\omega})|d\omega=\pi\sum_{i=1}^{n_\gamma}\ln|\gamma_i|\geq 0$*. Then as a fundamental limitation, it is inevitable that* $\exists\omega:|1-P_{d,L}(e^{j\omega})Q_L(e^{j\omega})|>1$*. For plants whose relative degree is zero, let* $\rho=\lim_{z\to\infty}P_{d,L}(z)$ *and note that* $\lim_{z\to\infty}Q_L(z)=gb_0(1-k_2)/2$*, then*

$$\sigma=\rho gb_0(1-k_2)/[2-\rho gb_0(1-k_2)],$$

and $\sigma+1=2/[2-\rho gb_0(1-k_2)]$*. When* $0<B_w<L/(4T_s)$*,* $\tan(\pi B_w T_s/L)\in(0,1)$ *and hence* $k_2\in(0,1)$ *in (7). Thus there always exists a* $g(>0)$ *such that* $\ln|\sigma+1|>0$*, leading to a relaxation of the waterbed effect.*

3.2. Multirate Model Based Prediction

In this subsection, design of the MMP block in Fig. 2 is provided, to establish the equivalence of the MR-FMDOB to the fast-rate FMDOB in Fig. 3.

Recall that the input to $Q_L(z)$ in Fig. 3 is an estimate of $d_L[n]$; while the input to MMP is the slow T_s–sampled $d[n]$. Similar to the fundamental limitation in reconstructing analog signals from its samples (cf. Section 1), if the sampling in $d[n]=d_c(nT_s)$ did not contain aliasing, perfect reconstruction of the fast T_s/L–sampled $d_L[n]$ for a general disturbance signal can only be achieved if MMP contains an upsampler and an acausal infinite-length interpolator in the form of an ideal low-pass filter (with DC gain L and cutoff frequency π/L) [6].

The next result shows that the above fundamental limitation can be overcame if $d_L[n]$ satisfies an internal signal model. Intuitively, with such a signal model, inter-sample values of the disturbance can be reconstructed by using the historical data. We first provide the general case of the multirate prediction, then present an example that specifically addresses prediction at a particular frequency.

Theorem 1. *Let $d[n] = d_c(nT_s)$ and $d_L[n] = d_c(nT_s/L)$. If there exists a polynomial $A(z^{-1}) = 1 + a_1 z^{-1} + a_2 z^{-2} + \dots a_m z^{-m}$ ($a_m \neq 0$) such that $A(z^{-1}) d_L[n] = 0$ at the steady state,[2] then $d_L[n]$ can be fully recovered from the slowly sampled $d[n]$ by*

$$d_L[nL] = d[n], \tag{14}$$

and for $k = 1, 2, \dots, L-1$,

$$\begin{aligned} d_L[nL+k] &= W_k(z^{-1}) d[n] \\ &= w_{k,0} d[n] + w_{k,1} d[n-1] + \dots + w_{k,n_{w_k}} d[n-n_{w_k}], \end{aligned} \tag{15}$$

where n_{w_k} is the order of $W_k(z^{-1})$.

The minimum required order for $W_k(z^{-1})$ is $n^*_{w_k} = m-1$, in which case the coefficients of $W_k(z^{-1}) = w_{k,0} + w_{k,1} z^{-1} + \dots + w_{k,m-1} z^{-m+1}$ come from the unique solution of

$$M_k \begin{bmatrix} f_{k,1} \\ \vdots \\ \dfrac{f_{k,L(m-1)-m+k}}{w_{k,0}} \\ \vdots \\ w_{k,m-1} \end{bmatrix} = - \begin{bmatrix} a_1 \\ a_2 \\ \vdots \\ a_m \\ 0 \\ \vdots \\ 0 \end{bmatrix}, \tag{16}$$

$$M_k \triangleq \left[\begin{array}{c|cccc} \tilde{M}_k & e_k & e_{k+L} & \dots & e_{k+(m-1)L} \end{array} \right] \tag{17}$$

$$\in \mathbb{R}^{[L(m-1)+k] \times [L(m-1)+k]}, \tag{18}$$

where e_j is the elemental column vector whose entries are all zero except for the j-th entry, which equals 1; and $\tilde{M}_k$ is

$$\tilde{M}_k \triangleq \begin{bmatrix} 1 & 0 & \dots & 0 \\ a_1 & \ddots & \ddots & \vdots \\ \vdots & \ddots & \ddots & 0 \\ a_m & \ddots & \ddots & 1 \\ 0 & \ddots & \ddots & a_1 \\ \vdots & \ddots & \ddots & \vdots \\ 0 & \dots & 0 & a_m \end{bmatrix}_{[L(m-1)+k] \times [L(m-1)-m+k]}. \tag{19}$$

Proof By definition, $d_L[nL] = d_c(nT_s) = d[n]$. Hence (14) holds. To establish (15), construct

$$\begin{aligned} &F_k(z^{-1}) A(z^{-1}) + z^{-k} W_k(z^{-L}) = 1, \\ &W_k(z^{-L}) \triangleq w_{k,0} + w_{k,1} z^{-L} + w_{k,2} z^{-2L} + \dots + w_{k,n_{w_k}} z^{-n_{w_k} L}, \\ &F_k(z^{-1}) \triangleq 1 + f_{k,1} z^{-1} + f_{k,2} z^{-2} + \dots + f_{k,n_{f_k}} z^{-n_{f_k}}, \end{aligned} \tag{20}$$

where $w_{k,n_{w_k}} \neq 0$, $f_{k,n_{f_k}} \neq 0$, and $W_k(z^{-L})$ is obtained by replacing each z^{-1} in $W_k(z^{-1})$ with z^{-L}. As $A(z^{-1}) d_L[n] = 0$ at steady state, it must be that $F_k(z^{-1}) A(z^{-1}) d_L[n] \to 0$, which gives, after substituting in (20),

$$(1 - z^{-k} W_k(z^{-L})) d_L[n] \to 0. \tag{21}$$

[2]Here, z^{-1} is a one-step delay operator such that $z^{-1} u[n] = u[n-1]$.

For $n = \tilde{n}L + k$ ($k \in \mathbb{Z}^+$, $k < L$), this implies that, at steady state,

$$\begin{aligned} d_L[\tilde{n}L+k] &= z^{-k} W_k(z^{-L}) d_L[\tilde{n}L+k] \\ &= w_{k,0} d_L[\tilde{n}L] + w_{k,1} d_L[(\tilde{n}-1)L] + w_{k,2} d_L[(\tilde{n}-2)L] + \\ &\qquad \dots + w_{k,n_{w_k}} d_L[(\tilde{n}-n_{w_k})L]. \end{aligned} \tag{22}$$

But by definition $d_L[(\tilde{n}-i)L] = d[\tilde{n}-i]$. Hence, with a change of notations, the result simplifies to the asserted (15).

Consider solving (20), which is a special constrained Diophantine equation. Matching the coefficients of z^{-i}'s ($i = 1$, 2,..., $m + n_f$), one can obtain $m + n_{f_k}$ linear equations with the $n_{f_k} + n_{w_k} + 1$ parameters of $F_k(z^{-1})$ and $W_k(z^{-L})$ as the unknowns. A solution thus exists if

$$n_{f_k} + n_{w_k} + 1 \geq m + n_{f_k}. \tag{23}$$

Additionally in (20), the highest order of z^{-1} must be the same in $F_k(z^{-1}) A(z^{-1})$ and $z^{-k} W_k(z^{-1})$, namely,

$$m + n_{f_k} = k + L n_{w_k}. \tag{24}$$

Hence the minimum-order solution is achieved with

$$n^*_{w_k} = m-1, \; n^*_{f_k} = L(m-1) - m + k. \tag{25}$$

Under (25), the coefficients of z^{-l}'s, $l \in \{1, 2, \dots, L(m-1)+k\}$, in $A(z^{-1}) F_k(z^{-1}) + z^{-k} W(z^{-L})$ are given by

$$\begin{aligned} &w_{k,p} + \sum_{i,j=0,1,\dots}^{i+j=pL+k} a_i f_{k,j} : \text{for } z^{-pL-k}, \; p = 0, 1, \dots, m-1 \\ &\sum_{i,j=0,1,\dots}^{i+j=l} a_i f_{k,j} : \text{for } z^{-l}, \; l \neq pL+k \; \forall p \in \{0, 1, \dots, m-1\}, \end{aligned}$$

where $f_{k,0} = 1$ and $a_0 = 1$. All the above coefficients must be zero for (20) to hold. Confining so yields, after some matrix algebra, (16). The column vectors of M_k in (17) are all linearly independent. Hence M_k is non-singular and a unique solution always exists. □

Transient response: It is recognized that $W_k(z^{-1})$ is a finite-impulse-response filter. The transient of the reconstruction process in (15) equals n_{w_k} discrete time steps, which is usually very fast compared to the transient of the feedback servo control.

Choice of L in practice is based on the engineering judgment between computation complexity and performance. With $L \to \infty$ and proper design of the fast-sampled Q filter, the compensation approximates a continuous-time perfect disturbance cancellation scheme. However, increasing L will linearly increase the number of unknowns in the matrix equation (16). Also, as $L \to 0$, digital controllers can become highly sensitive to round-off errors under finite arithmetic implementation [2].

Corollary 1. *$\forall \phi \in \mathbb{R}$ and $1/(2T_s) < \Omega_o < 1/T_s$, let $d_c(t) = \cos(2\pi\Omega_o t + \phi)$. Let the analog signal be sampled at T_s, i.e., Ω_o is in between the Nyquist frequency and the sampling frequency. The beyond-Nyquist information can be fully recovered by letting $\omega_o = 2\pi\Omega_o T_s/L$, $L = 2$, and reconstructing the T_s/L-sampled $d_L[n] = \cos(\omega_o n + \phi)$ with*

$$d_L[2n] = d[n] = d_c(nT_s), \tag{26}$$

$$d_L[2n+1] = \left(2\cos\omega_o - \frac{1}{2\cos\omega_o} \right) d[n] - \frac{1}{2\cos\omega_o} d[n-1]. \tag{27}$$

Proof Ω_o is below the new Nyquist frequency corresponding to the sampling time of $T_s/2$. Based on Shannon's sampling theory, $L=2$ is sufficient for $d_L[n]$ to recover the analog information. For $d_L[n]=\cos(\omega_o n+\phi)$, we have, from the table of Z transform,

$$d_L[n]=\frac{(1-z^{-1}\cos\omega_o)\cos\phi-z^{-1}\sin\omega_o\sin\phi}{1-2z^{-1}\cos\omega_o+z^{-2}}\delta[n];$$

and hence $A(z^{-1})=1+a_1z^{-1}+a_2z^{-2}=1-2\cos\omega_o z^{-1}+z^{-2}$, as $A(z^{-1})d_L[n]=(1-z^{-1}\cos\omega_o)\cos\phi\delta[n]-\sin\omega_o\sin\phi\delta[n-1]=0\ \forall n\geq 2$. Apply Theorem 1 with $m=2$ in $A(z^{-1})$ and $L=2$. Only one intersample point needs to be reconstructed, i.e., $k=1$ in (15). The constrained Diophantine equation becomes

$$A(z^{-1})F(z^{-1})+z^{-1}W(z^{-2})=1, \tag{28}$$

and (16) is

$$\left[\begin{array}{c|cc} 1 & 1 & 0 \\ a_1 & 0 & 0 \\ a_2 & 0 & 1 \end{array}\right]\left[\begin{array}{c} f_1 \\ \hline w_0 \\ w_1 \end{array}\right]+\left[\begin{array}{c} a_1 \\ a_2 \\ 0 \end{array}\right]=\left[\begin{array}{c} 0 \\ 0 \\ 0 \end{array}\right], \tag{29}$$

which gives $d_L[2n+1]=w_0d[n]+w_1d[n-1]$ in (27). □

Significance and implications: The key in the multirate prediction is the construction and solution of (20). Under the original steady-state disturbance model $A(z^{-1})d_L[n]=0$, we have $d_L[n]=-a_1d_L[n-1]-a_2d_L[n-2]+\ldots a_md_L[n-m]$, i.e., the historical data at a sampling time of T_s/L must be available to predict $d_L[n]$. With (20) and the resulting (22), we have expanded the prediction horizon and scattered the distance between the required historical data by exactly L samples.

With a proper choice of L in Corollary 1 and Theorem 1, the T_s-sampled $d[n]$ can practically recover the full information of $d_L[n]$ as if the analog signal is $d_c(t)$ is sampled at T_s/L. When T_s/L is small enough such that the corresponding Nyquist frequency ($\pi L/T_s$ rad) is above the spectrum of $d_c(t)$, fast control can accommodate the recovered signal at a conventionally unattainable frequency.

Implementation: For implementation, a proper L is firstly chosen based on the criteria in the last paragraphs. (16) is solved for each k to yield the linear predictors $\{W_k(z^{-1})\}_{k=1}^{L-1}$ (15) for the $L-1$ intersample points between $d[n]$ and $d[n+1]$. Note that the dimensions of M_k are different for each k; yet, the order of $W_k(z^{-1})$ is the same. Hence a shared memory of $d[n]$,..., $d[n-n_{w_k}]$ can be used when predicting $\{d_L[nL+k]\}_{k=1}^{L-1}$. In more details, we have:

procedure MMP(T_s, L, $A(z^{-1})$)
  for $k=1,2,\ldots,L-1$ **do**
    Form (19) and (17); solve (16) for $W_k(z^{-1})$ in (15).
  end for
  Implement $W_k(z^{-1})$ at each intersample instance.
end procedure

3.3. Integrated FMDOB and MMP

Given the baseline sampling time T_s sec and the beyond-Nyquist target frequency $\Omega_0>1/(2T_s)$, after combining the last two subsections, we have the following implementation steps for the MR-FMDOB algorithm.

procedure MR-FMDOB(T_s, Ω_o, $P(s)$ or $P_{d,L}(z^{-1})$, $A(z^{-1})$)
  Design L; ensure $L/(2T_s)>\Omega_0$.
  Implement **Procedure** MMP.
  Obtain $P_{d,L}(z^{-1})$, ZOH of $P(s)$ w.r.t. T_s/L.
  Let $\omega_o=2\pi\Omega_oT_s/L$.
  Obtain $|P_{d,L}(e^{j\omega_o})|$ and $\varphi\triangleq$ phase $\left(P_{d,L}(e^{j\omega_o})\right)$.
  Design k_2 based on (7); start with a value very close to one (e.g. between 0.95 and 0.995) for good robustness.
  Compute (5) and (6) at T_s/L. Define $Q_L(z^{-1})$ in (4).
  Implement Fig. 2.
end procedure

4. Numerical Verification

Consider a plant $P_c(s)=3.74488\times10^9\mathrm{e}^{-0.01s}/(s^2+565.5s+319775.2)$, which is the model of a high-precision linear stage used in semiconductor manufacturing. Let the sampling time be limited at $T_s=1/2640$ second, and the baseline discrete-time controller be a PID controller $C(z)=k_p+k_i/(z-1)+k_d(z-1)/z$ with $k_p=1/13320$, $k_i=1/33300$, and $k_d=1/2775$. Plotting the closed-loop discrete-time sensitivity function reveals that such a baseline design provides a common discrete-time loop shape with sufficient gain and phase margins.

Continuous-time vibrations are applied to the plant, above Nyquist frequency. For convenience of illustration, we denote Ω_N(=1320 Hz) as the Nyquist frequency. To see the limitation (and danger) of sub-Nyquist design in this case, the narrowband disturbance observer [31] is applied on top of the PID controller, to enable infinite-gain control at selective frequencies below Ω_N. Such a design provides perfect compensation of sinusoidal signals below Nyquist frequency, and is termed 1x compensation. Fig. 4 presents the corresponding plant output. When the disturbance occurs at 2376 Hz (i.e. $1.8\Omega_N$), although the sub-Nyquist servo enhancement enforces the T_s-sampled output to converge to zero in Fig. 4a, the actual output is significantly amplified. The 3σ (σ is the standard deviation) value of the $T_s/2$-sampled output increased from 15.71 to 20.96, yielding more than 130% of error amplification. To reveal more details in the error amplification, Fig. 4c shows the spectrum of the output sampled at $T_s/2$ sec. Two peaks are present in each spectral plot: the second revealing the energy of the actual disturbance; while the first—symmetric to the second peak with respect to Ω_N—comes from the aliased disturbance component below Nyquist frequency [6]. After aliasing below Nyquist frequency, the two peaks with opposite phase values are canceled to yield the deceiving zero steady state value in Fig. 4a. Yet, the output energy in the top plot of Fig. 4c is actually increased, as the sub-Nyquist design did not target at the true disturbance spectrum beyond Ω_N.

In Table 1, a series of disturbances at frequencies between Ω_N and $2\Omega_N$ are applied to the plant. Based on the 3σ value of the output, the largest servo degradation under sub-Nyquist high-gain control occurred when the disturbance frequency is closest to the Nyquist frequency, where the tracking errors get amplified by 165.12% compared to the baseline value.

Fig. 5 shows the efficiency of the proposed algorithm in rejecting the beyond-Nyquist disturbances. As the disturbance

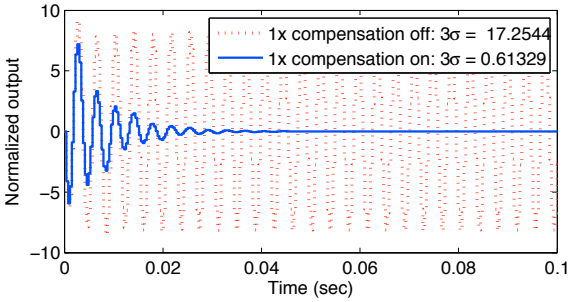

(a) output sampled at T_s.

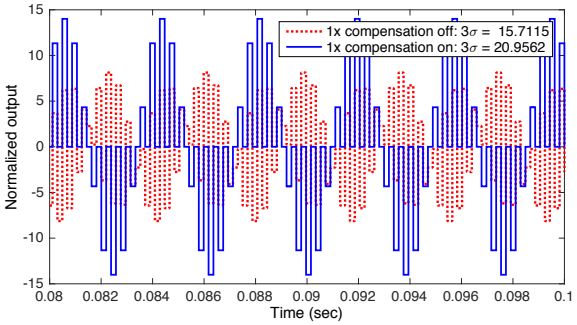

(b) output sampled at $T_s/2$.

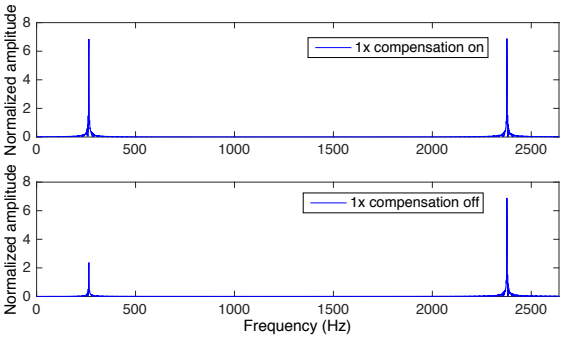

(c) Fast Fourier Transform (FFT) of $y_c(t)$ sampled at $T_s/2$.

Figure 4: Plant output for the case with disturbance at $1.8\Omega_N$.

Table 1: Servo degradation w.r.t. different disturbances: $y_c(t)$ sampled at $T_s/20$.

disturbance frequency	3σ value of y		amplification
	1x compensation		
	off	on	
$1.3\Omega_N$	14.76	24.37	165.12%
$1.7\Omega_N$	15.25	21.01	137.72%
$1.8\Omega_N$	15.71	20.96	133.38%
$1.9\Omega_N$	17.39	20.94	120.38%

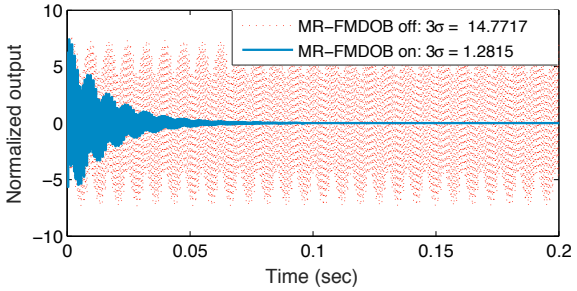

(a) $y_c(t)$ sampled at $T_s/2$.

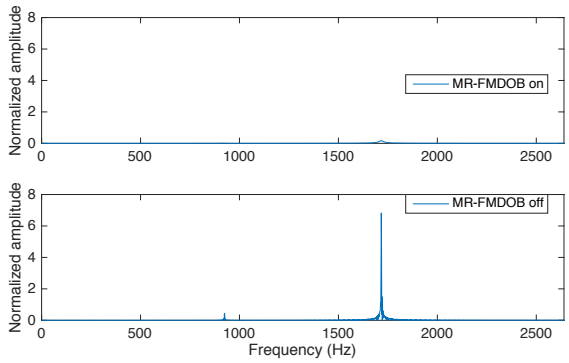

(b) FFT of $y_c(t)$ sampled at $T_s/2$.

Figure 5: Plant output under MR-FMDOB, for the case with disturbance at $1.3\Omega_N$.

lies in $(\Omega_N, 2\Omega_N)$, $L = 2$ was adopted in the upsampler of MR-FMDOB. Under the worst-case disturbance profile in Table 1, the $T_s/2$-sampled outputs were significantly improved compared to the baseline results. At the steady state, the $T_s/2$-sampled output in Fig. 5a converged to zero. The overall (including the transient response) 3σ value of the output was reduced by 91.32%—in contrast to the 165.12% amplification in Table 1. In the frequency domain, it is also seen from Fig. 5b, that the actual disturbance spectrum is significantly attenuated at the correct frequency location (cf. Fig. 4c). Analogous verifications were performed on all the cases in the table, where the proposed algorithm achieved a consistent performance improvement of over 91% 3σ reduction in all cases. In all cases, the same values of design parameters are used [$k_2 = 0.9765$ (corresponding to $B_w = 20$ Hz in $Q_L(z)$), $L = 2$, $g = 1$].

Fig. 6 shows an example of the time-domain signal recovery by the MMP algorithm. Here, the actual harmonic disturbance is plotted in $*$ at a fast sampling time of $T_s/2$; the measured signal is plotted in the solid black line marked by circles. Under the limited sensing, the MMP successfully reconstructed the hidden fast data (marked in rectangular) at the intersample instances.

5. Conclusion and Discussions

In this paper, the problem of sampled-data regulation control against structured disturbances beyond Nyquist frequency is addressed. Based on models of the plant and the disturbance, a multirate forward-model disturbance observer is proposed to enable full rejection of beyond-Nyquist vibration disturbances at an arbitrary selection of uniformly distributed inter-sample instances.

The proposed algorithm is intrinsically of add-on nature, and can be placed in an existing regular discrete-time servo loop. Certainly, sampled-data control can not perfectly reject a continuous-time disturbance. In practice, engineering judgements must be performed to decide a suitable upsampling ratio

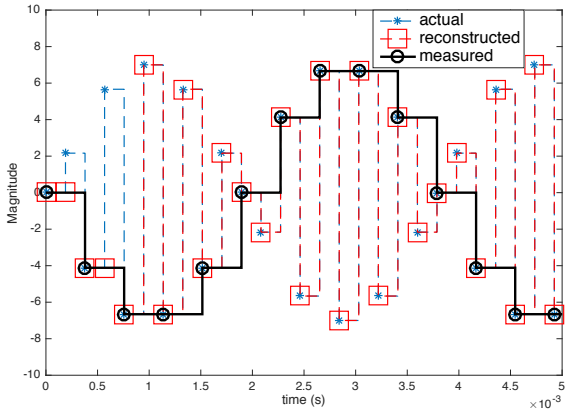

Figure 6: Time trace of MMP based data recovery.

L, such that the major disturbance components are covered under the new servo capabilities.

Although only one harmonic disturbance is included in the example, the algorithm is directly extendible to disturbances with multiple harmonics. T_s, L, and $A(z^{-1})$—the inputs to the MMP procedure in Section 3.2—are not restricted to the case of single harmonic functions. When there are $p \in \mathbb{Z}^+$ frequency components $\{\bar{\Omega}_i\}_{i=0}^{p-1}$ in the disturbance, one can set $A(z^{-1}) = \prod_{i=0}^{p-1}(1-2\cos(2\pi\bar{\Omega}_i T_s/L)z^{-1}+z^{-2})$. Correspondingly, for the FMDOB, one lets $\Omega_o = \bar{\Omega}_i$ and applies the procedure of Section 3.3 for each $\bar{\Omega}_i$, to obtain $Q_L(\bar{\Omega}_i, z)$, and then forms $Q_L(z) = \sum_{i=0}^{p-1} Q_L(\bar{\Omega}_i, z)$ by superposition. It is recommended to set k_2 very close to one in each $Q_L(\bar{\Omega}_i, z)$, such that the summation preserves the nominal shape of a scaled band-pass filter.

References

[1] W. E. Frazier, "Metal additive manufacturing: A review," *J. Mater. Eng. Perform.*, vol. 23, no. 6, pp. 1917–1928, 2014.

[2] B. Bamieh, "Intersample and finite wordlength effects in sampled-data problems," *IEEE Trans. Autom. Control*, vol. 48, no. 4, pp. 639–643, Apr. 2003.

[3] D. Hu and R. Kovacevic, "Sensing, modeling and control for laser-based additive manufacturing," *Int. J. of Mach. Tools and Manufacture*, vol. 43, no. 1, pp. 51 – 60, 2003.

[4] D. Hu, M. Labudovic, and R. Kovacevic, "On-line sensing and estimation of laser surface modification by computer vision," *Proc. Institution of Mech. Engineers, Part B: J. of Eng. Manufacture*, vol. 215, no. 8, pp. 1081–1090, 2001.

[5] C. E. Shannon, "Communication in the Presence of Noise," *Proc. IRE*, vol. 37, no. 1, pp. 10–21, 1949.

[6] A. V. Oppenheim and R. W. Schafer, *Discrete-Time Signal Processing (3rd Edition)*, 3rd ed. Prentice Hall, Aug. 2009.

[7] Y. Yamamoto, M. Nagahara, and P. P. Khargonekar, "Signal Reconstruction via H-infinity Sampled-Data Control Theory—Beyond the Shannon Paradigm," *IEEE Trans. Signal Process.*, vol. 60, no. 2, pp. 613–625, Jan. 2012.

[8] M. Unser, "Sampling-50 years after Shannon," *Proc. IEEE*, vol. 88, no. 4, pp. 569–587, 2000.

[9] H. Fujimoto and Y. Hori, "High-performance servo systems based on multirate sampling control," *Control Eng. Practice*, vol. 10, no. 7, pp. 773–781, 2002.

[10] T. Oomen, J. van de Wijdeven, and O. Bosgra, "Suppressing intersample behavior in iterative learning control," *Automatica*, vol. 45, no. 4, pp. 981–988, Apr. 2009.

[11] T. Sato and S. MasudaMember, "Generalized predictive control for improving intersample performance," *IEEJ Trans. Electr. Electron. Eng.*, vol. 2, no. 6, pp. 620–626, Nov. 2007.

[12] S. Hara, M. Tetsuka, and R. Kondo, "Ripple attenuation in digital repetitive control systems," in *Proceedings of IEEE Conference on Decision and Control*, Dec. 1990, pp. 1679–1684 vol.3.

[13] T. Atsumi, "Disturbance suppression beyond Nyquist frequency in hard disk drives," *Mechatronics*, vol. 20, no. 1, pp. 67–73, Feb. 2010.

[14] A. Feuer and G. Goodwin, "Generalized sample hold functions-frequency domain analysis of robustness, sensitivity, and intersample difficulties," *IEEE Trans. Autom. Control*, vol. 39, no. 5, pp. 1042–1047, May 1994.

[15] B. Friedland, "Sampled-data control systems containing periodically varying members," in *Proc. 1st IFAC congress*. Moscow: Butterworths Scientific Publishers, 1960, pp. 139–146.

[16] A. Tangirala, S. Shah, and T. Chen, "Conditions for removing intersample ripples in multirate control," in *1999 IEEE Canadian Conference on Electrical and Computer Engineering*, vol. 3, May 1999, pp. 1585–1589 vol.3.

[17] G. C. Goodwin and A. Feuer, "Linear periodic control: A frequency domain viewpoint," *Systems & Control Letters*, vol. 19, no. 5, pp. 379–390, Nov. 1992.

[18] H. Fujioka and S. Hara, "Output regulation for sampled-data feedback systems: Internal model principle and H_∞ servo controller synthesis," *Proc. IEEE Conf. Decision and Control*, pp. 4867–4872, 2006.

[19] D. Youla, J. J. Bongiorno, and H. Jabr, "Modern wiener–hopf design of optimal controllers part i: The single-input-output case," *IEEE Trans. Autom. Control*, vol. 21, no. 1, pp. 3–13, 1976.

[20] V. Kucera, "Stability of discrete linear feedback systems," in *Proc. 6th IFAC World Congress, paper 44.1*, vol. 1, 1975.

[21] R. Kalman, Y. Ho, and K. Narendra, "Contributions to Differential Equations," *New York, NY, USA: Interscience*, vol. 1, no. 2, pp. 189–213, 1963.

[22] T. Chen and B. A. Francis, *Optimal Sampled-Data Control Systems*. Springer, Oct. 2013.

[23] B. A. Francis and T. Georgiou, "Stability theory for linear time-invariant plants with periodic digital controllers," *IEEE Trans. Autom. Control*, vol. 33, no. 9, pp. 820–832, 1988.

[24] R. Middleton and J. Freudenberg, "Non-pathological sampling for generalized sampled-data hold functions," *Automatica*, vol. 31, no. 2, pp. 315 – 319, 1995.

[25] C. E. Garcia and M. Morari, "Internal model control. A unifying review and some new results," *Ind. & Eng. Chemistry Process Design and Develop.*, vol. 21, no. 2, pp. 308–323, Apr. 1982.

[26] B. D. Anderson, "From youla kucera to identification, adaptive and nonlinear control," *Automatica*, vol. 34, no. 12, pp. 1485 – 1506, 1998.

[27] M. Bodson, "Rejection of periodic disturbances of unknown and time-varying frequency," *International Journal of Adaptive Control and Signal Processing*, vol. 19, no. 2-3, pp. 67–88, Mar. 2005.

[28] P. Regalia, "An improved lattice-based adaptive IIR notch filter," *IEEE Trans. Signal Process.*, vol. 39, no. 9, pp. 2124–2128, 1991.

[29] P. Regalia, S. Mitra, and P. Vaidyanathan, "The digital all-pass filter: A versatile signal processing building block," *Proc. IEEE*, vol. 76, no. 1, pp. 19–37, 1988.

[30] B.-F. Wu and E. Jonckheere, "A simplified approach to bode's theorem for continuous-time and discrete-time systems," *IEEE Trans. Autom. Control*, vol. 37, no. 11, pp. 1797–1802, Nov 1992.

[31] X. Chen and M. Tomizuka, "A minimum parameter adaptive approach for rejecting multiple narrow-band disturbances with application to hard disk drives," *IEEE Trans. Control Syst. Technol.*, vol. 20, no. 2, pp. 408–415, March 2012.